Journal of Solid State Chemistry 182 (2009) 203–207

Contents lists available at ScienceDirect

Journal of Solid State Chemistry

journal homepage: www.elsevier.com/locate/jssc

Rapid Communication

Novel powellite-based red-emitting phosphors: $CaLa_{1-x}NbMoO_8:xEu^{3+}$ for white light emitting diodes

Mariyam Thomas, P. Prabhakar Rao *, M. Deepa, M.R. Chandran, Peter Koshy

Materials and Minerals Division, National Institute for Interdisciplinary Science and Technology (NIIST), Trivandrum 695 019, India

ARTICLE INFO

Article history:
Received 11 June 2008
Received in revised form
6 October 2008
Accepted 11 October 2008
Available online 1 November 2008

Keywords:
Molybdate
Powellite
Red-emitting phosphor
WLED

ABSTRACT

We report the photoluminescence properties of a novel powellite-based red-emitting phosphor material: $CaLa_{1-x}NbMoO_8:xEu^{3+}$ (0.01, 0.03, 0.05, 0.1) for the first time. The photoluminescence investigations indicated that $CaLa_{1-x}NbMoO_8:xEu^{3+}$ emits strong red light at 615 nm originating from $^5D_0 \rightarrow {}^7F_2$ (electric dipole transition) under excitation either into the $^5L_0$ state with 394 nm or the $^5D_2$ state with 464 nm, that correspond to the two popular emission lines from near-UV and blue LED chips, respectively. When compared with emission intensity from a $CaMoO_4:Eu^{3+}$, the emission from $CaLaNbMoO_8:Eu^{3+}$ showed greater intensity values under the same excitation wavelength (394 nm). The enhanced red emission is attributed to the enhanced *f–f* absorption of Eu^{3+}. These materials could be promising red phosphors for use in generating white light in phosphor-converted white light emitting diodes (WLEDs).

© 2008 Elsevier Inc. All rights reserved.

1. Introduction

White light emitting diodes (WLEDs) have got much attention in recent years because of their wide applications as well as their advantages over conventional light sources. High color rendering index (CRI), long life time, high luminescence efficiency, low power consumption, environment friendly are some of the advantages of white LEDs [1,2]. There are several approaches in developing white LEDs. One approach for producing white light is the combination of blue InGaN chip (λ_{em}~(450–470 nm) with yellow phosphor such as YAG:Ce^{3+} [3]. However, this type of white light has poor CRI because of the color deficiency in the red and green region. To improve the CRI, then a variety of other approaches for white light generation were realized, such as by the pumping of red, green and blue phosphors with a ultraviolet (UV) LED (λ_{em}~370–410 nm) or by using a blue LED in conjunction with green ($SrGa_2S_4:Eu^{2+}$) and red ($SrY_2S_4:Eu^{2+}$) phosphors [4]. In these approaches, the combination of a near-UV LED and the tri-color phosphors may be the most convenient way to obtain high quality WLEDs. The current phosphor materials used for solid-state lighting based on near-UV InGaN-based LEDs (λ_{em}~370–410 nm) are $BaMgAl_{10}O_{17}:Eu^{2+}$ for blue, $ZnS:Cu^{2+}$, Al^{3+} for green and $Y_2O_2S:Eu^{3+}$ for red and that for blue LED chip, the phosphors are $SrGa_2S_4:Eu^{2+}$ for green and $SrY_2S_4:Eu^{2+}$ for red [5]. However, the sulfide-based red phosphors have some drawbacks such as poor absorbance near-UV region, lack of chemical stability, decomposition products (such as sulfide gas, which is harmful to the environment). Therefore, it is necessary to develop novel, stable, and efficient red phosphors for LED applications that can be effectively excited in the near-UV region. In this regard, many red phosphors having scheelite-, westfieldite-, and oxyapatite-related structures have been investigated [6–11]. Among these, molybdates and tungstates with scheelite structure are considered as good host lattice under near-UV or blue excitation due to its MoO_4 tetrahedron unit [12]. These materials have broad and intense charge transfer (CT) absorption bands in the UV and therefore capable of efficiently capturing the emission from a GaN-based LED over a range of wavelength. However, these materials have relatively weak absorption near-UV and blue region and further they need high doping concentration of activator (24 mol% Eu^{3+}) for the strong emission [2]. To overcome some of these problems, Wang et al. co-doped Sm^{3+}, Bi^{3+} and Eu^{3+} in molybdates and enhanced emission intensity of Eu^{3+} [13]. However, more efficient red phosphors are needed to achieve an acceptable efficiency of WLED.

Recently, we could prepare some new powellite type phases, $CaRENbMoO_8$ (RE = Y, La, Nd, Sm or Bi) [14] and it is found that when doped with Eu^{3+} in $CaLaNbMoO_8$, they give strong red emission spectra under near-UV or blue excitation wavelength. When compared with emission intensity from a $CaMoO_4:Eu^{3+}$, the emission from $CaLaNbMoO_8:Eu^{3+}$ showed greater intensity values under the near-UV excitation wavelength. Some of our results on photoluminescence properties of these new materials are presented in this paper.

* Corresponding author. Fax: +91 471 2491712.
E-mail address: padala_rao@yahoo.com (P. Prabhakar Rao).

0022-4596/$ - see front matter © 2008 Elsevier Inc. All rights reserved.
doi:10.1016/j.jssc.2008.10.015

2. Experimental

2.1. Preparation of $CaLa_{1-x}NbMoO_8:xEu^{3+}$ (0.01, 0.03, 0.05, 0.1) samples

Novel powellite-based red-emitting phosphors with the general composition: $CaLa_{1-x}NbMoO_8:xEu^{3+}$ were prepared by solid-state reaction using $CaCO_3$, La_2O_3, Nb_2O_5, MoO_3, and Eu_2O_3 (All chemicals are from Acros Organics with 99.9% purity) as the starting materials. The required stoichiometric amounts of these materials were weighed and then thoroughly wet mixed in an agate mortar with acetone as the wetting medium. The mixing is followed by drying in an air oven. The mixing and drying was repeated thrice to obtain a homogenous mixture. The obtained mixture was initially calcined at 1100 °C for 6 h in a platinum crucible in an air atmosphere furnace. The calcination was repeated thrice with intermittent grinding. The samples calcined at 1100 °C were analyzed by X-ray diffraction (XRD) for the phase identification. It was observed that a major phase of powellite type of $CaMoO_4$ was formed along with a small amount of fergusonite type phase of $LaNbO_4$. The calcination was repeated at 1200 °C for 6 h in order to obtain a single phase.

2.2. Characterization

The crystal structure as well as the phase purity of the calcined samples was identified by recording the powder XRD patterns using Philip's X'Pert diffractometer with Ni filtered Cu$K\alpha$1 radiation ($\lambda = 1.54056$ Å). The data were recorded over the 2θ range of 10°–80° with a step width of 0.08°. The particle size and morphology of the powder samples were studied by scanning electron microscope (SEM) (JEOL, JSM-5600 LV). The UV-vis absorption of the samples was recorded by UV-vis spectrophotometer (Shimadzu UV-2401). Excitation and emission spectra were recorded using a Spex-Fluorolog DM3000F spectrofluorimeter and a 450 W xenon flash lamp as the exciting source.

3. Results and discussion

3.1. Powder XRD studies

Fig. 1 shows the powder X-ray diffraction patterns of the $CaLa_{1-x}NbMoO_8$: xEu^{3+} ($x = 0.01$, 0.03, 0.05, 0.1) phosphors. The obtained patterns were found to be similar to that of the earlier reported for $CaMoO_4$ [14]. All the peaks in the XRD patterns are indexed with the $CaMoO_4$ (JCPDS file no. 29-0351) tetragonal powellite structure with the space group $I4_1/a$. The prominent peaks correspond to (112), (004), (200), (204), (220), (116) and (312) lattice planes [14]. The sharp and intense peaks of the patterns indicate the crystalline nature of the samples. The structure refinement of all the XRD patterns for $CaLa_{1-x}NbMoO_8$: xEu^{3+} was further performed by the Rietveld analysis using the X'pert plus program which was done as follows: the starting model for the refinement of the phases was taken from the reported crystal structure of $CaMoO_4$ in which Ca and La/Eu are at (4*b*: 0, 1/4, 5/8) sites, Nb and Mo at (4*a*: 0, 1/4, 1/8) sites and O at (16*f*: *x*, *y*, *z*), $Z = 4$ in the space group $I4_1/a$, no. 88 [12,15]. The profile was fitted using Pseudo-Voigt profile function. Fig. 2 shows the typical best fit that was observed, calculated, the difference powder diffraction profiles and the expected Bragg reflections for $CaLa_{0.97}Eu_{0.03}NbMoO_8$. The *R*-factors, the refined oxygen coordinates, thermal displacement parameters, the lattice parameters and other parameters obtained from the Rietveld refinement of the powder diffraction data for all the compositions are given in Table 1. The refined *R*-values suggest that the refinement is in good agreement with the space group in all respects. It can be seen from the refined cell parameters that the lattice parameters decrease with the increase of Eu^{3+} concentration as expected, since the ionic radius of Eu^{3+} ($r = 0.107$ nm, when coordination number (CN) = 8) is smaller than that of the La^{3+} ($r = 0.116$ nm, when CN = 8). This further confirms that substitution of Eu^{3+} takes place in the lattice site of La^{3+}. (The lattice parameters for $CaMoO_4$ with tetragonal structure are $a = 0.5226$ nm and $c = 1.143$ nm [16]).

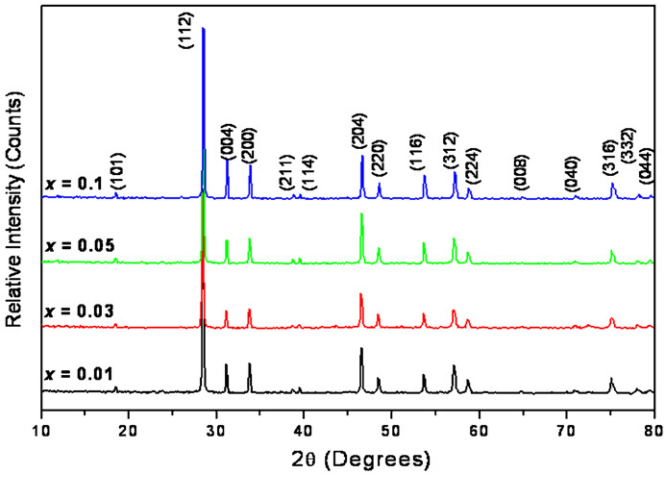

Fig. 1. Powder X-ray diffraction patterns of $CaLa_{1-x}NbMoO_8:xEu^{3+}$ ($x = 0.01$, 0.03, 0.05, 0.1).

3.2. SEM studies

Fig. 3 shows the typical SEM micrographs of all the Eu^{3+}-doped samples. The powder particles appear to be highly crystalline and are slightly agglomerated. The extent of crystalline and de-agglomeration is observed with the increase of europium concentration in the host. The particles are in the scale of 1–7 μm in size with homogenous nature.

3.3. Photoluminescent studies

The UV-vis absorption spectra of the host material and that of $CaLa_{0.95}NbMoO_8:0.05Eu^{3+}$ is presented in Fig. 4. The absorption

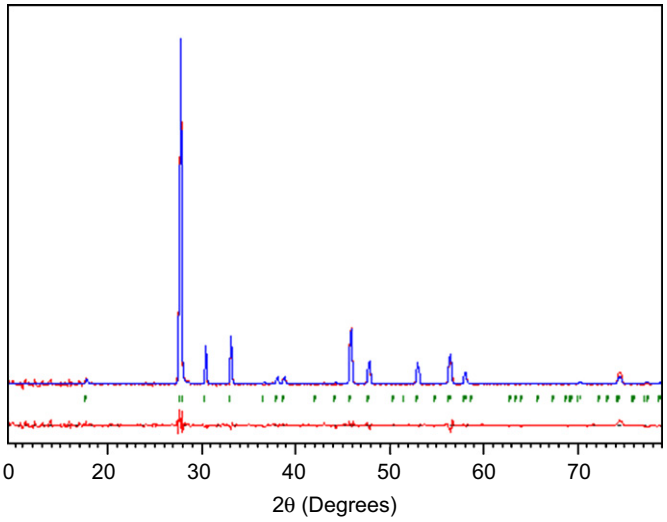

Fig. 2. Observed (red), calculated (blue) and difference (red) powder X-ray diffraction profiles obtained from the Rietveld refinement of powder X-ray diffraction data for $CaLa_{0.97}Eu_{0.03}NbMoO_8$. The expected Bragg peak positions are marked below the profile fit as vertical bars.

Table 1
Variation of lattice parameters, oxygen coordinates, *R*-factors, isotropic thermal displacement parameters and other parameters obtained from Rietveld analysis of the $CaLa_{1-x}NbMoO_8:xEu^{3+}$.

x:	0.01	0.03	0.05	0.1
Lattice parameters				
a (nm)	0.53200 (6)	0.53199 (5)	0.53167 (7)	0.53107 (7)
c (nm)	1.15250 (1)	1.15200 (1)	1.15140 (2)	1.15010 (2)
Oxygen position coordinates				
x	0.1499 (1)	0.1490 (9)	0.1499 (9)	0.1499 (9)
y	0.0069 (9)	0.0069 (7)	0.0069 (7)	0.0069 (9)
z	0.2099 (5)	0.2099 (1)	0.2099 (5)	0.2099 (1)
Residues				
$R_{p\ (\%)}$	9.37	6.15	5.19	9.66
$R_{wp\ (\%)}$	15.68	9.41	9.41	12.52
$R_{exp\ (\%)}$	12.50	11.58	8.67	9.47
$R_{B\ (\%)}$	3.39	3.07	4.34	4.51
Thermal parameter, B_{iso} (Å^2)				
Ca	0.8799 (9)	0.8799 (9)	0.8799 (9)	0.8799 (9)
La	0.8799 (9)	0.8799 (9)	0.8799 (9)	0.8799 (9)
Eu	0.8799 (9)	0.8799 (9)	0.8799 (9)	0.8799 (9)
Nb	0.5 (1)	0.5 (1)	0.5 (1)	0.5 (1)
Mo	0.5 (1)	0.5 (1)	0.5 (1)	0.5 (1)
O	1.0199 (1)	1.0199 (1)	1.0199 (1)	1.0199 (1)
2θ data range (°)	10–80	10–80	10–80	10–80
Step size (°)	0.08	0.08	0.08	0.08
Total number of reflections	28	28	28	28
Number of reflections resolved	16	16	16	16
Number of intensity dependent parameters	12	12	12	12

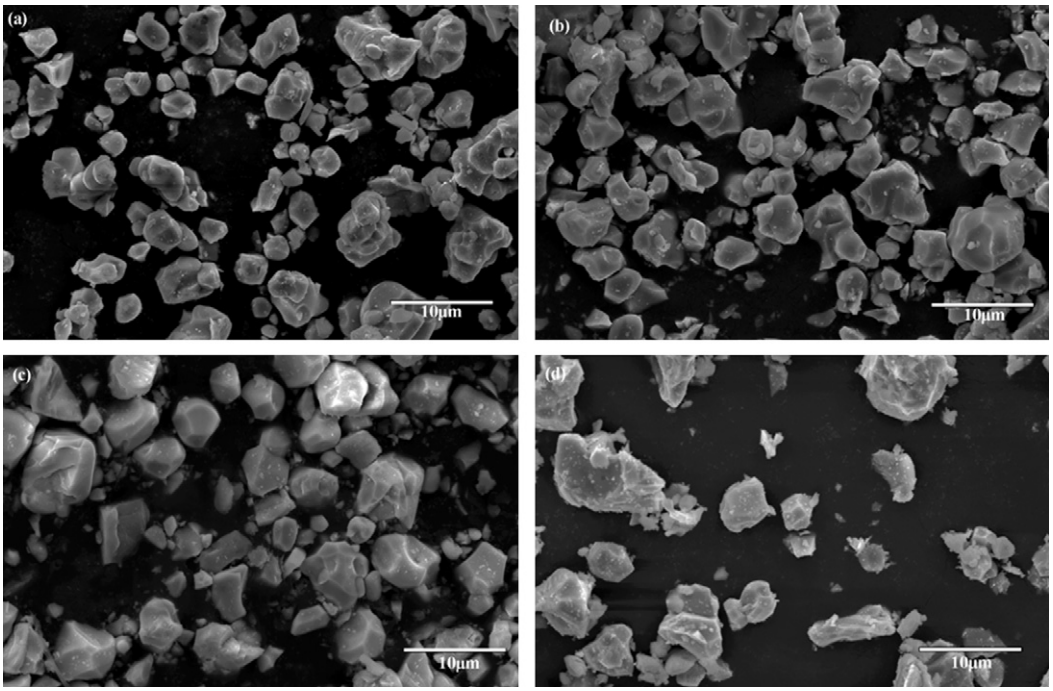

Fig. 3. Scanning electron micrographs of phosphor powders of $CaLa_{1-x}NbMoO_8:xEu^{3+}$ with varying Eu^{3+} concentrations: (a) $x = 0.01$, (b) $x = 0.03$, (c) $x = 0.05$, and (d) $x = 0.1$.

spectra of $CaLaNbMoO_8$ exhibits a strong absorption band around 277 nm in the UV region which is mainly attributed to the CT from the oxygen ligand to the central molybdenum and niobium atom inside MoO_4 and NbO_4 groups, respectively. The $0.05Eu^{3+}$-doped sample shows the absorption peaks of the intra-4*f* transitions of Eu^{3+} at 394 and 464 nm (enlarged view of the wavelength region

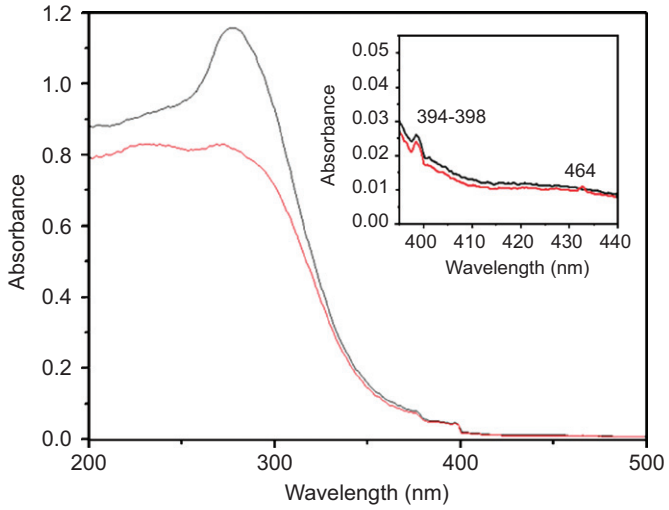

Fig. 4. UV-vis absorption spectra of $CaLa_{1-x}NbMoO_8$:xEu^{3+} ($x = 0$, 0.05). The inset shows an enlarged view of the wavelength region between 390 and 470 nm.

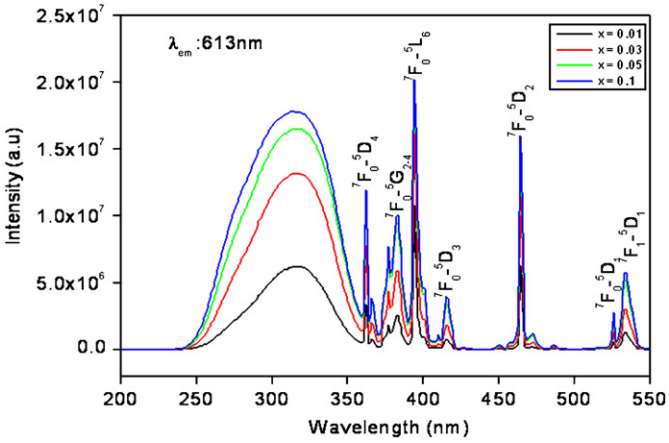

Fig. 5. Excitation spectra of $CaLa_{1-x}NbMoO_8$:xEu^{3+} ($x = 0.01$, 0.03, 0.05, 0.1) for an emission at 613 nm.

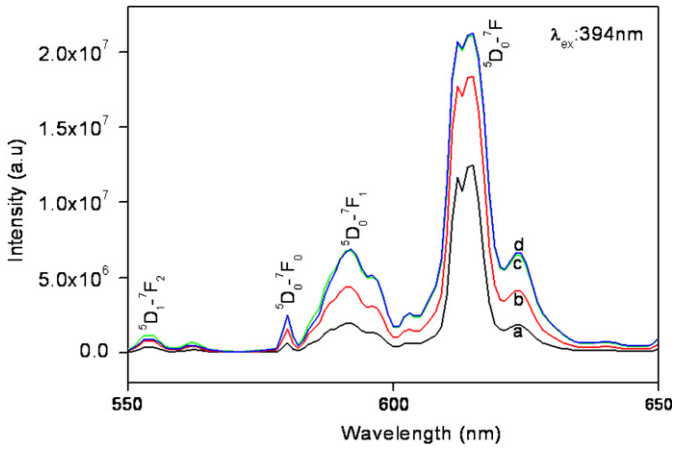

Fig. 6. Emission spectra of $CaLa_{1-x}NbMoO_8$:xEu^{3+} with varying Eu^{3+} concentrations: (a) $x = 0.01$, (b) $x = 0.03$, (c) $x = 0.05$, and (d) $x = 0.1$ under 394 nm excitation.

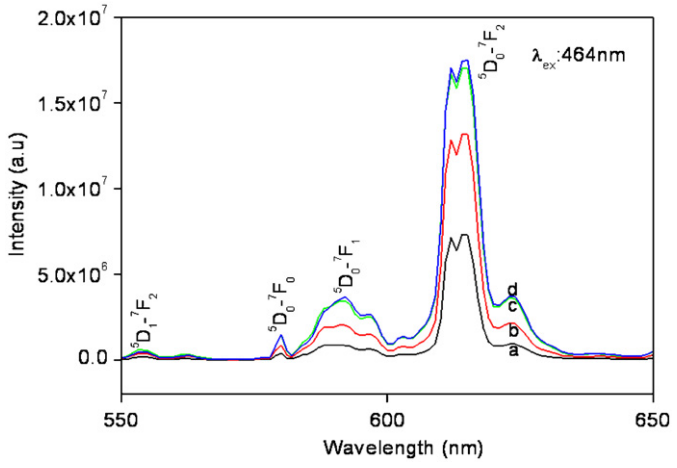

Fig. 7. Emission spectra of $CaLa_{1-x}NbMoO_8$:xEu^{3+} with varying Eu^{3+} concentrations: (a) $x = 0.01$, (b) $x = 0.03$, (c) $x = 0.05$, and (d) $x = 0.1$ under 464 nm excitation.

between 390 and 470 nm is shown in the inset of Fig. 4) in addition to the CT absorption band of the host and the O^{2-}–Eu^{3+} in the UV region. Both the samples have the strong absorption edge near-UV around 350 nm. It can be seen from the Fig. 4 that the intensity of absorbance for $CaLaNbMoO_8$ is greater than that of the europium-doped sample indicating the energy conversion from the CT states to the Eu^{3+} emitting levels is efficiently taking place.

Fig. 5 shows the excitation spectra of $CaLa_{1-x}NbMoO_8$:xEu^{3+}($x = 0.01$, 0.03, 0.05, 0.1). The excitation spectra include a broad region (240–350 nm) followed by a series of sharp peaks beyond 350 nm. It has been reported that the excitation spectra of $CaMoO_4$:$0.05Eu^{3+}$ shows a dominant broad band, which corresponds to the combination of CT transitions from Eu^{3+}–O^{2-} and $(MoO_4)^{2-}$ groups [1,16]. Also $LaNbO_4$ shows strong absorbance at 260 nm corresponding to the CT band in NbO_4 group [17]. It can be assumed that the observed broad band in the present excitation spectra corresponds to the combinations of the CT transitions from Eu^{3+}–O^{2-}, $(MoO_4)^{2-}$ and NbO_4 groups. The sharp peaks above 350 nm are due to the intra-configurational (f–f) transitions of Eu^{3+}, including the peaks with maxima at 362 nm ($^7F_0$–$^5D_4$), 384 nm ($^7F_0$–$^5G_{2-4}$), 394 nm ($^7F_0$–$^5L_6$), 412 nm ($^7F_0$–$^5D_3$), 464 nm ($^7F_0$–$^5D_2$), 525 nm ($^7F_0$–$^5D_1$), and 533 nm ($^7F_0$–$^5D_1$), respectively [18,19]. Among them, the intensity of the peaks at 394 and 464 nm excitation wavelengths (which are emission wavelengths of near-UV and blue LED chips, respectively), is much stronger than the other transitions of Eu^{3+}. This implies that these samples can be effectively excited by radiations of wavelength in the near-UV and blue regions. It is also observed that the absorption peaks of intra-4f transitions of Eu^{3+} increase with increasing concentration of europium, which evidences that the enhancement of emission of Eu^{3+} is caused mainly by the increase absorption of strength of $^7F_0$–$^5L_6$ and $^7F_0$–$^5D_2$ transitions.

Figs. 6 and 7 show the emission spectra of $CaLa_{1-x}NbMoO_8$:xEu^{3+}($x = 0.01$, 0.03, 0.05, 0.1) for two excitation wavelengths 394 and 464 nm, respectively. The major emission peaks are observed at 580, 591, 612, 615, 623 nm. All these are characteristic emission peaks of Eu^{3+} ion and are corresponding to ^5D_J ($J = 0$, 1)-^7F_J ($J = 1$, 2, 3, 4) transitions [12]. Of these peaks, the red emission peaks at 612 and 615 nm are more dominant than the other peaks. The two red peaks at 612 and 615 nm are due to the Eu^{3+} electric dipole transitions of $^5D_0$–$^7F_2$, which indicates that Eu^{3+} occupies a non centro-symmetric site [20]. These transitions are generally forbidden since the parity doesn't allow these transitions. The emission corresponding to the orange region (590 nm) is weak, which are assigned to the magnetic dipole transitions $^5D_0$–$^7F_1$ and

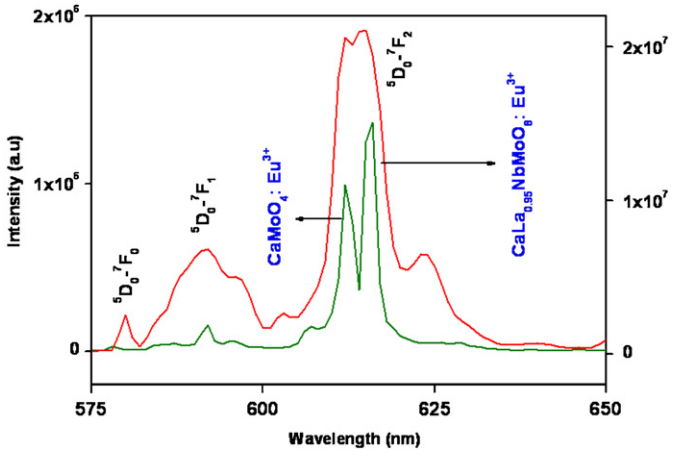

Fig. 8. Comparison of emission spectra of: (a) CaMoO4:0.05Eu^{3+} and (b) $CaLa_{0.95}NbMoO_8$:0.05Eu^{3+} under 394 nm excitation.

are insensitive to the site symmetry [16]. The emission lines are similar for the excitation wavelengths, 394 and 464 nm. However, it is seen that the red emission intensity excited at near-UV radiation (394 nm) is greater than that of the emission excited at blue region 464 nm. From Figs. 4 and 5, it is also observed that with the increase of Eu^{3+} concentration, the intensities of all the emission lines are enhanced significantly and reaching a maximum at a concentration of 5 mol% and remains almost same for 10 mol% of europium. Thus concentration quenching occurs in this case and the optimum concentration for maximum intensity is between 5 and 10 mol% of europium. It is well known that lower doping concentrations of activator (Eu^{3+}) lead to weak luminescence, while higher doping concentrations cause quenching of the luminescence of Eu^{3+} [20]. This is known as concentration quenching. Self quenching is known in many other hosts and is associated with exchange interactions. It can also be noted that the full width half maximum (FWHM) of the red peak increases with the increase of the doping concentration of Eu^{3+} up to $x = 0.05$, then remains the same at 10 mol% of Eu^{3+}. This observation can also be attributed to concentration quenching. It should be mentioned here that charge compensation approach and high doping concentrations of europium (24 mol%) are required in $CaMoO_4$:Eu^{3+} red phosphor in order to get reasonable emission intensity [21]. In the present $CaLa_{1-x}NbMoO_8$:xEu^{3+} phosphor, europium ion (Eu^{3+}) is expected to replace La^{3+} in order to maintain the charge balance in the lattice. Further, high red emission intensity values are achievable with 5 mol% of europium concentration.

With the purpose of red phosphor application for white light LEDs with near-UV/blue GaN-based chips as excitation source, the emission spectra of $CaLaNbMoO_8$:0.05Eu^{3+} and $CaMoO_4$:0.05Eu^{3+} under the same excitation of 394 nm radiation (near-UV) are compared as shown in Fig. 8. As can be seen from this figure, the FWHM of the emission peaks of $CaLa_{0.95}NbMoO_8$:0.05Eu^{3+} is larger than the FWHM of emission peaks of $CaMoO_4$:0.05Eu^{3+}. This is probably due to the fact that the number of Eu^{3+} spectroscopic sites (different surroundings) for $CaLa_{0.95}NbMoO_8$:0.05Eu^{3+} is greater than the number of Eu^{3+} spectroscopic sites for $CaMoO_4$:0.05Eu^{3+}. Further it is observed that the red emission intensity of $CaLaNbMoO_8$:0.05Eu^{3+} is about ten times stronger than that of $CaMoO_4$:0.05Eu^{3+}. It has been reported earlier that $CaMoO_4$:Eu^{3+} emits stronger red fluorescence than CaS:Eu^{3+} phosphor used in white light LEDs. And also, the strong red emission results from the high doping concentration of Eu^{3+} (about 24 mol%) [2]. This clearly demonstrates that the present 5 mol% Eu^{3+} is a promising red phosphor for white LEDs.

4. Conclusion

In summary, a novel powellite-based red-emitting phosphor, $CaLaNbMoO_8$:xEu^{3+} has been investigated for the first time. The photoluminescent properties of $CaLaNbMoO_8$:xEu^{3+} indicate that these samples exhibit enhanced red emission of Eu^{3+} (615 nm) under the excitation of near-UV 394 nm and blue light 464 nm that correspond to the two popular emission lines from near-UV and blue LED, respectively. The enhanced red emission is attributed to the enhanced *f–f* absorption of Eu^{3+}. The most efficient concentration for the maximum emission occurs between 5 and 10 mol% of Eu^{3+}, with red emission stronger than $CaMoO_4$:Eu^{3+} phosphor. Therefore, it can be concluded that the Eu^{3+}-doped $CaLaNbMoO_8$ under the excitation of near-UV 394 nm radiations could be a promising red phosphor for applications in WLEDs.

References

[1] Y. Hu, W. Zhuang, H. Ye, J. Lumin. 111 (2005) 139.
[2] S. Yan, J. Zhang, X. Zhang, J. Phys. Chem. C 111 (2007) 13256.
[3] S. Nakamura, G. Fasol, The Blue Laser Diodes, GaN Based Light Emitters and Lasers, Springer, Berlin, 1997, p. 216.
[4] Y. Huh, J. Park, S. Kweon, J. Kim, Y. Rag Do, Bull. Korean Chem. Soc. 25 (2004) 1585.
[5] T. Nishida, T. Ban, N. Kobayashi, Appl. Phys. Lett. 82 (2003) 3817.
[6] J.S. Kim, P.E. Jeon, J.C. Choi, H.L. Park, S.I. Mho, G.C. Kim, Appl. Phys. Lett. 84 (2004) 2931.
[7] F.N. Shi, J. Meng, Y.F. Ren, J. Mater. Chem. 7 (1997) 773.
[8] S. Neeraj, N. Kijima, A.K. Cheetham, Chem. Phys. Lett. 387 (2004) 2.
[9] J.G. Wang, X.P. Jing, C.H. Yan, J.H. Lin, J. Electrochem. Soc. 152 (2005) G186.
[10] J.P.M. Van Vliet, G. Blasse, L.H. Brixner, J. Solid State Chem. 76 (1988) 160.
[11] K.-S. Sohn, J.M. Lee, N. Shin, Adv. Mater. 15 (2003) 2081.
[12] Z.J. Zhang, H.H. Chen, X. Yang, J. Zhao, Mater. Sci. Eng. B 145 (2007) 34.
[13] Z. Wang, H. Liang, M. Gong, Q. Su, Opt. Mater. 29 (2006) 896.
[14] K. Ravindran Nair, P. Prabhakar Rao, S. Sameera, V.S. Mohan, M.R. Chandran, P. Koshy, Mater. Lett. 62 (2008) 2868.
[15] S.N. Achary, S.J. Pawte, M.D. Mathews, A.K. Tyagi, J. Phys. Chem. Solids 67 (2006) 774.
[16] Y. Hu, W. Zhuang, H. Ye, J. Alloys Compd. 390 (2005) 226.
[17] Y.J. Hsiao, T.H. Fang, Y.S. Chang, Y.H. Chang, C.H. Liu, L.W. Ji, W.Y. Jywe, J. Lumin. 126 (2007) 866.
[18] S.M. Thomas, P. Prabhakar Rao, K. Ravindran Nair, P. Koshy, J. Am. Ceram. Soc. 91 (2) (2008) 473.
[19] J. Wang, X. Jing, C. Yan, J. Lina, J. Electrochem. Soc. 152 (3) (2005) G186.
[20] G. Blasse, Chemistry and physics of *R*-activated phosphors, in: K.A. Gschneider Jr., L. Eyring (Eds.), Handbook on the Physics and Chemistry of Rare-Earths, North-Holland, Amsterdam, 1979.
[21] J. Liu, H. Lian, C. Shi, Opt. Mater. 29 (2007) 1591.